Development of an Adaptive Approach for Precision Agriculture Monitoring with Drone and Satellite Data

Deepak Murugan, Akanksha Garg, and Dharmendra Singh, *Senior Member, IEEE*

***Abstract*—For better agricultural productivity and food management, there is an urgent need for precision agriculture monitoring at larger scales. In recent years, drones have been employed for precision agriculture monitoring at smaller scales, and for past few decades, satellite data are being used for land cover classification and agriculture monitoring at larger scales. The monitoring of agriculture precisely over a large scale is a challenging task. In this paper, an approach has been proposed for precision agriculture monitoring, i.e., the classification of sparse and dense fields, which is carried out using freely available satellite data (Landsat 8) along with drone data. Repeated usage of drone has to be minimized and hence an adaptive classification approach is developed, which works with image statistics of the selected region. The proposed approach is successfully tested and validated on different spatial and temporal Landsat 8 data.**

***Index Terms*—Adaptive thresholding, drone, Landsat 8, precision agriculture monitoring, satellite images, unmanned aerial vehicle.**

I. Introduction

AGRICULTURE has a prime role in the Indian economy, as it shares about 17% of GDP and employs about 50% of the workforce. For better agricultural production and for food management, providing key ideas through precision agriculture monitoring is important. Precision agriculture is a crop management concept that is field specific and is more helpful for better productivity. Precision agriculture [1], [2] makes use of real-time information from sensors and geospatial techniques (remote sensing, geographic information system) and helps in making smarter decisions for better productivity. The use of wireless sensor networks for precision agriculture is widely discussed in [3] and [4], which employs wireless sensors directly in the field to collect and transmit information to data processing center through network. Usage of drones or unmanned aerial vehicle for precision agriculture [5] is the latest trend. With the easy availability of commercial drones at affordable costs, farmers can use them for monitoring their farms. However, in countries like India, where all cannot afford such monitoring system, people are still dependent on the physical inspection of the crops. Thus, a solution at global level is required and satellite images are widely used for the same. Fusion of satellite image with drone image for precision agriculture monitoring is an important task to be explored.

Land-cover classification [6] into classes like water, vegetation, bare land, urban, etc., is researched for many years and several supervised and unsupervised classification approaches are available, such as decision tree, neural network [7], object-based image analysis [8], support vector machine, and time-series analysis [9]. Crop-type classification with the help of spectral signatures from hyperspectral images [10], [11] and temporal signatures from time-series multispectral images [12] has also been carried out by many researchers. Satellite images are also downscaled to provide better spatial resolution and some of the commonly used downscaling techniques are probabilistic model based [13], sensor based [14], learning based [15], scaling laws [16], frequency representation, and panchromatic sharpening [17].

Satellite images are used for applications such as the identification of sparse shrublands and sparse grasslands for desertification monitoring [18] with the accuracy of 79% and 66%, respectively; quantifying sparse vegetation cover with mixture modeling using aircraft-based Probe-1 hyperspectral imagery [19], etc. However within class classification such as the segregation of vegetation regions into sparse and dense regions in a large field using satellite imagery, a part of precision agriculture monitoring has not been explored yet. There is a need for precision agriculture monitoring at large scale and synergetic use of satellite data along with drone imagery [20] might help solve such problems, as drone images can provide precise ground truth information. Researchers have used only drone images for precision agriculture monitoring applications like crop biomass monitoring [21], water stress in crops [22], detecting small weed patches [23], for mapping vineyard vigor [24], and for examining the results of various nitrogen treatments on crops [25]. In all these approaches, we have to fly a drone every time to obtain the results. Therefore, emphasis was on carrying out fusion of drone and satellite data only once, and then use satellite data alone for other locations/data without the requirement of drone images.

The main aim of this paper is to develop such a technique by which the repetitive usage of drone can be minimized without

Manuscript received March 13, 2017; revised June 22, 2017 and August 7, 2017; accepted August 15, 2017. This work was supported in part by RailTel and in part by the Indian Council of Agricultural Research. *(Corresponding author: Dharmendra Singh.)*

The authors are with the Department of Electronics and Communication Engineering, Indian Institute of Technology Roorkee, Roorkee 247667, India (e-mail: mdeepakiitr@gmail.com; akanksha126@gmail.com; dharmendrasing@yahoo.com).

Color versions of one or more of the figures in this paper are available online at http://ieeexplore.ieee.org.

Digital Object Identifier 10.1109/JSTARS.2017.2746185

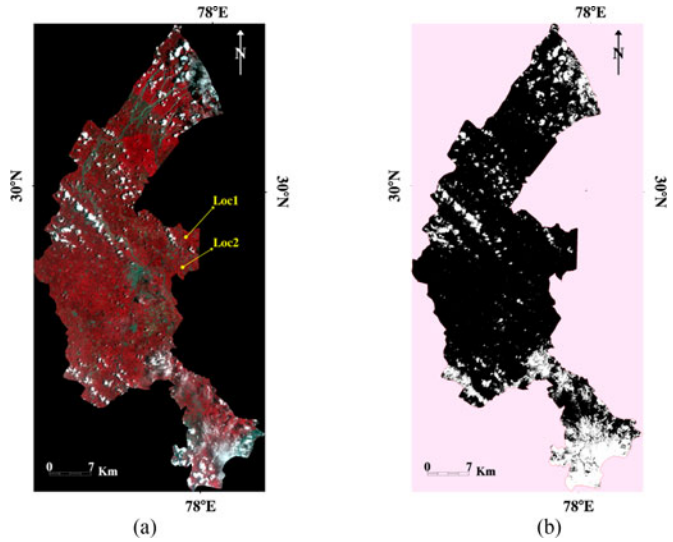

Fig. 1. Landsat 8 data (L8A) of Roorkee Tehsil: (a) FCC (NIR, red, and green), and (b) cloud mask (white represents clouded data).

affecting the end results of precision agriculture monitoring. For this purpose, we have developed an adaptive thresholding approach with the help of fusion of satellite (Landsat 8) and drone data. After the development of the methodology, we can directly use the satellite data without the requirement of drone data for the similar type of field.

This paper is organized as follows: In Section II, description of study area and data used is mentioned. Section III provides the model development and implementation approach. The results of the developed approach and their comprehensive analysis are presented and discussed in Section IV. Finally, the concluding remarks are given in Section V.

II. Study Area and Data Used

A. Study Area

Agriculture fields around Roorkee in Haridwar district, Uttarakhand, India are chosen as study area for this study. Sugarcane is one of the most prominent crops cultivated in the district of Haridwar, and more than 50% of the cultivable area in this district is used for sugarcane cultivation.

B. Data Used

In this study, multispectral satellite data downloaded from the United States Geological Survey and drone image acquired during visits in the field are used.

1) Landsat 8 Data: Landsat 8 multispectral data have 11 spectral bands, with a spatial resolution of 30 m and revisit time of 16 days. Data are available in the form of tiles and the tile selected for this study covers Haridwar district of Uttarakhand, India, along with some parts of neighboring districts. Fig. 1(a) shows a false color composite (FCC) image of Landsat 8 data of Roorkee Tehsil with near-infrared (NIR), red, and green bands, and the two study areas are marked as Loc1 and Loc2. Details of Landsat 8 tiles used are listed in Table I. Landsat data downloaded are stored as quantized and calibrated digital numbers

TABLE I
Details of Landsat 8 Data Used

S. No.	Id.	Data Id	Date of Acquisition
1	L8A	LC81460392016174LGN00	June 22, 16
2	L8B	LC81460392016206LGN00	July 24, 16

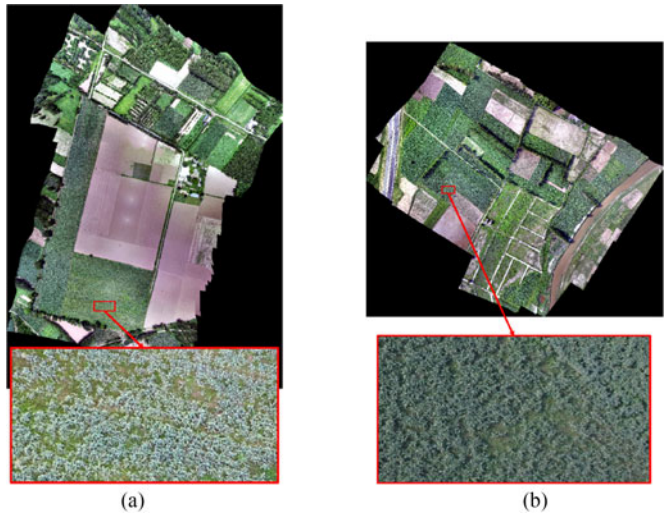

Fig. 2. Mosaic of drone images from (a) Loc1B (inset: highly sparse region), and (b) Loc2A (inset: moderate sparse region).

TABLE II
Details of Drone Data Used

S. No.	Id.	DOA	Central Lat	Central Lon
1	Loc2A	June 29, 2016	29°53'13.88"N	77°57'27.14"E
2	Loc1B	August 9, 2016	29°55'50.49"N	77°57'51.47"E

(DN). Spectral reflectance [26] is obtained from the DN using (1) with coefficients provided in metadata file:

$$\rho = M_\rho . Q_{\text{cal}} + A_\rho \tag{1}$$

where ρ is the spectral reflectance, M_ρ is the reflectance multiplicative factor from the band, A_ρ is the reflectance additive factor, and Q_{cal} is the pixel value in DN.

2) Drone Image: Drone image acquired using a DJI phantom quadcopter over the selected agriculture field is used for this study. The drone has a high definition 4K resolution RGB camera with an attached GPS unit to capture geotagged RGB images. Two agricultural fields were selected and the drone was flown at a height of 100 m above ground level to capture images. Images were captured over the agriculture field in such a way that there is at least 40% overlap between two consecutive images. The acquired images are mosaicked, orthorectified, and georegistered for the two locations, as shown in Fig. 2(a) and (b). The spatial resolution of mosaicked drone images is 6 cm. Table II presents the list of date of acquisition (DOA) of drone images along with their location Id and coordinates. The date at which drone images were captured are chosen to be close to Landsat acquisition date over the selected test site.

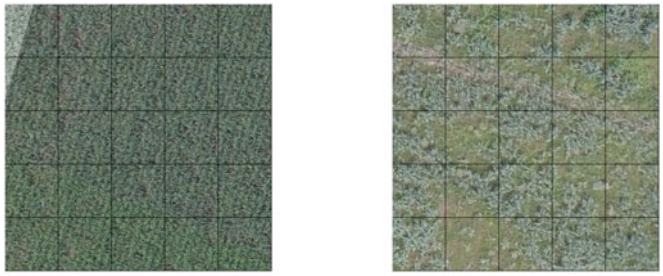

Fig. 3. Drone image segments with 5×5 grids overlaid: (a) dense segment, and (b) sparse segment.

III. Model Development and Implementation

The aim of this approach is to distinguish sparse and dense vegetation within a large agriculture field. For developing this approach, only sugarcane fields are considered, and various steps used were critically analyzed and performed, which are described in the following subsections.

A. Cloud Masking

Optical data are generally affected by cloud. For applications such as agriculture monitoring, which is to be performed in real-time, only the images available could be used. But using cloud-affected data might lead to misleading information due to altered reflectance values. So, there is a need to mask cloud-affected data before proceeding for further analysis. Landsat 8 data are provided with a quality assessment band, which consist of 16 flag bits. High state i.e., '1' in the 14^{th} and 15^{th} flag bits indicates the presence of a cloud in the selected pixel, and the mask is thus created using this information, as shown in Fig. 1(b). The obtained mask is verified with the mask obtained using cloud detection technique described in [27]. The percentage of cloud-affected area for Roorkee Tehsil in data L8A and L8B were found out to be 17.6% and 7.8%, respectively. It is observed that subset of L8A data for Loc1 had cloud-affected pixels in it. Since L8B data are not affected by cloud and Loc1 sugarcane field having similar proportion of sparse and dense areas, drone data Loc1B and Landsat data L8B are used for initial analysis.

B. Drone Image Segmentation and Gridding

Subset image from drone image is cropped with the help of upper left and lower right coordinates obtained from Landsat data subset. The spatial resolution of drone data is 6 cm and that of Landsat data is 30 m. Segments of $30\,\mathrm{m} \times 30\,\mathrm{m}$ are made out of drone image with the same area corresponding to each pixel of Landsat data subset. This is achieved by using the corresponding coordinates of each Landsat pixel as a center coordinate of each drone segment and segmenting it by selecting the required number of pixels around it. Similarly, the whole drone image subset is segmented into $30\,\mathrm{m} \times 30\,\mathrm{m}$ segments corresponding to the Landsat data. Grids of 5×5 are made over each of the drone image segment, which corresponds to $6\,\mathrm{m} \times 6\,\mathrm{m}$ in ground resolution for each grid. Fig. 3(a) and (b) shows gridded segments of dense and sparse locations, respectively, of the same field.

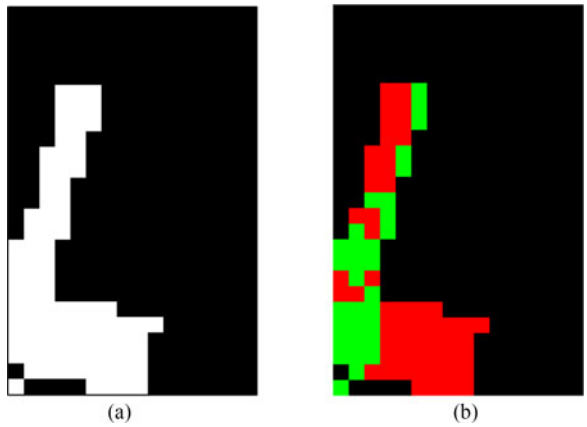

Fig. 4. Results for Loc1B of L8B subset: (a) vegetation mask (white represents sugarcane crop), and (b) classified image with sparse (red) and dense (green) areas.

C. Vegetation Extraction

In this paper, sugarcane fields are the main area of interest. During field survey, areas of sugarcane field are marked and verified with drone images. The segments obtained by the procedure discussed in Section III-B are used for the selection of pixels in the Landsat image. Vegetation (sugarcane) mask is thus obtained by selecting all pixels in the Landsat image that corresponds to sugarcane, as shown in Fig. 4(a). Using the obtained mask, the spectral information of all the sugarcane pixels in the Landsat data is extracted for further analysis.

D. Ground Truth Data Collection

With the help of the mask obtained, the percentage of dense vegetation area for sugarcane segments has to be computed. Regions with sparse sugarcane plantations have been marked on the basis of ground survey data and careful inspection of drone image. Using the grids shown in Fig. 3, each grid is marked as sparse or dense regions. There are total 25 grids in each segment and the percentage of dense area is then computed using the following equation:

$$\%\ \text{Dense area} = \frac{\text{Total no. of dense grids}}{25} \times 100 \qquad (2)$$

Segments with percentage dense area below 70% are assigned as sparse segments [28]. A total of 71 segments are present, of which approximately 47 segments are sparse and remaining 24 are dense segments. Fifteen segments of most sparse and most dense segments are chosen based on their dense area percentage and used as ground truth data for further analysis.

E. Band Selection for Sparse and Dense Classification

Once the sparse and dense segments are chosen from the drone image, its corresponding spectral reflectance values for bands green, red, NIR, SWIR1, SWIR2, and NDVI (normalized difference vegetation index) are extracted from the Landsat data. Mean and standard deviation for both the classes are computed for the selected six bands. Separability index (SI) [7], a measure used to identify the class separability, is used to identify the band that is best suitable for segregation of sparse and dense

classes and is computed using the following equation:

$$\mathrm{SI}_{i,j} = \frac{|\mu_i - \mu_j|}{\sigma_i + \sigma_j} \tag{3}$$

where μ and σ are the statistical mean and standard deviation of classes i and j, respectively. For a band if the SI value is greater than 1.5, it is suitable for the classification of the two classes. SI for SWIR1 band $(1.57\text{–}1.65\,\mu\mathrm{m})$ was found to be 2.50 [29], which was best among all other bands, and hence provides better separability. In addition to this, the reflectance at SWIR1 band decreases due to the absorption of incident energy by leaf moisture content [30]. Hence, in dense vegetated area the absorption is more, thus decrease in reflectance value and vice versa, which affirms our selection of the band.

F. Adaptive Thresholding

Once the band for classification is selected, there is a need to classify the data into two classes, sparse and dense vegetation by thresholding. Otsu thresholding [31] is applied for obtaining the threshold value th in [29]. The main drawback of this technique is that ground truth data, which is obtained from the drone image, are mandatory information for each area of interest that is to be classified. It is not possible to fly the drone each time over the area of interest, and hence an adaptive technique is required, which can handle the change in spatial and temporal variation of the image. In order to overcome this problem, an adaptive thresholding method [32], [33] is used. To identify the sparse region in the vegetation for precision monitoring of a particular field, we have applied gridding as discussed in Section III-B and sparse region is computed using (2). Then, we have assessed the overall accuracy (OA) on the basis of how many sparse grids over the sparse region are identified by the proposed algorithm. To obtain the sparse segment in the Landsat image, we have proposed an adaptive thresholding technique that is discussed in the following subsection.

1) Proposed Adaptive Thresholding Technique: The threshold (th) is calculated as follows:

$$th = \mu + n\sigma \tag{4}$$

where μ and σ are the mean and standard deviation of all the vegetation pixels in the image, respectively, and n (usually varied from -1 to 1 in steps of 0.1) is an unknown term whose value is selected in such a way that the two classes are classified with maximum accuracy. Two performance metrics, such as overall accuracy (OA) and false alarm rate (FAR), are used to determine the correctness of the value of n obtained as given in the following equations:

$$\mathrm{OA} = \frac{\text{No. of correctly detected sparse pixels}}{\text{Total no. of sparse pixels}} \tag{5}$$

$$\mathrm{FAR} = \frac{\text{No. of dense pixels classified as sparse}}{\text{Total no. of pixels - Total no. of sparse pixels}} \tag{6}$$

The plots of OA and FAR versus threshold (th) obtained from (4) for different values of n are shown in Fig. 5(a) and (b), respectively. From the plot, it is observed that the OA and FAR decrease with increasing threshold values as the sparse class lies to the right side of the mean image value. To determine an optimized threshold th, a mathematical formulation of both the curves is made using the curve fitting technique as

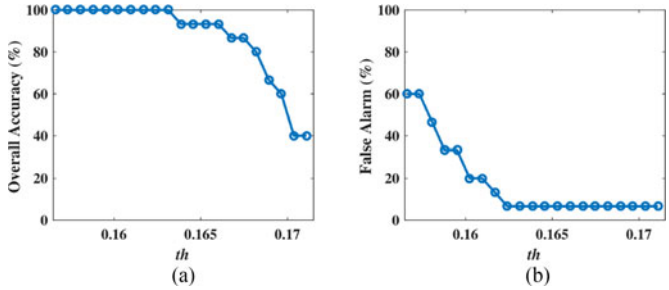

Fig. 5. Performance plot of varying values of th against (a) OA, and (b) FAR.

$$\mathrm{OA}(th) = -5.09e^{-16}e^{204th} + 0.1834e^{10.58th} \tag{7}$$

$$\mathrm{FAR}(th) = 8.737e^{19}e^{-297th} + 3e^{5}e^{-94.08th} \tag{8}$$

The goodness of fit of the curves estimated is tested using the *R*-squared (regression coefficient) estimate and it is found to be 0.976 and 0.968 for $\mathrm{OA}(th)$ and $\mathrm{FAR}(th)$ respectively, which indicates that there is a good fit between the obtained and original curves. It is necessary to maximize OA and minimize FAR for a better classification, which can be achieved by optimizing (7) and (8) for th. In order to make the algorithm image statistics dependent (adaptive), *th* in (7) and (8) is replaced with the expression in (4). Now, the OA and FAR are defined in terms of μ, σ, and n, which are given as follows:

$$\mathrm{OA}(n) = -5.09e^{-16}e^{204(\mu+n\sigma)} + 0.1834e^{10.58(\mu+n\sigma)} \tag{9}$$

$$\mathrm{FAR}(n) = 8.737e^{19}e^{-297(\mu+n\sigma)} + 3e^{5}e^{-94.08(\mu+n\sigma)} \tag{10}$$

Now, the problem is changed to determine the optimum value in terms of n. This is achieved using the multiobjective optimization approach and can be formulated as

$$\min\ f(n) = \begin{cases} f_1(n) \\ f_2(n) \end{cases}$$

where

$$f_1(n) = -f_{\mathrm{OA}}(n)$$
$$f_2(n) = f_{\mathrm{FAR}}(n)$$

subject to

$$f_{\mathrm{OA}}(n) \geq \mathrm{lb}_{\mathrm{OA}}$$
$$f_{\mathrm{FAR}}(n) \leq \mathrm{ub}_{\mathrm{FAR}}, \qquad -1 \leq n \leq 1 \tag{11}$$

Two constraints as given in (11) must be satisfied for the obtained optimal solution of n. The constraints are also user defined, i.e., it can be modified by users if in case no optimal solution is found for the default bounds (i.e., $\mathrm{lb}_{\mathrm{OA}}$ and $\mathrm{ub}_{\mathrm{FAR}}$). Default lower bound on OA ($\mathrm{lb}_{\mathrm{OA}}$) and upper bound on FAR ($\mathrm{ub}_{\mathrm{FAR}}$) to obtain optimal solutions are selected as 80% and 5%, respectively.

Fig. 6 shows the flowchart of the proposed methodology.

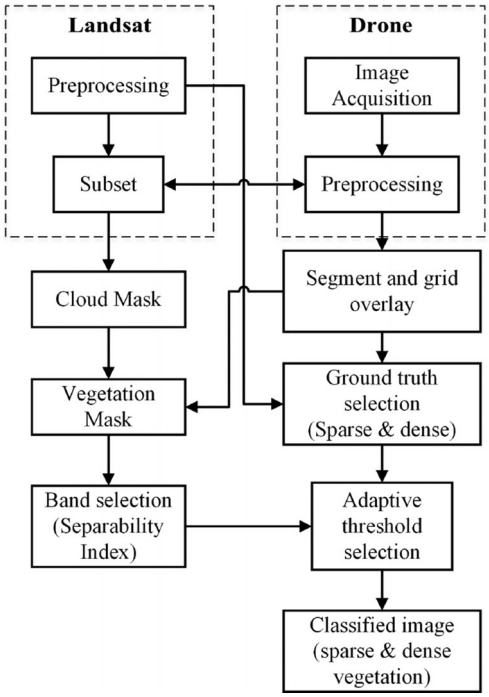

Fig. 6. Flowchart of the proposed methodology.

TABLE III
CONFUSION MATRIX FOR LOC1B OF L8B DATA

	Sparse#	Dense#	Total#	User Accuracy
Sparse#	36	5	41	87.80%
Dense#	4	26	30	86.66%
Total#	40	31	71	
Producer accuracy	90%	83.87%		
OA	62/71	87.32%		
FAR	5/31	16.13%		

Number of pixels.

TABLE IV
PERCENTAGE ERROR OF OMISSION AND COMMISSION FOR LOC1B OF L8B DATA

Class	Omission			Commission		
	Total Pixels	Pixels Omitted	Error %	Total Pixels	Pixels Commissioned	Error %
Sparse	40	4	0.1	41	5	0.12
Dense	31	5	0.16	30	4	0.13

IV. RESULTS AND DISCUSSION

A. Implementation Results

Landsat data are preprocessed and cloud-affected pixels are masked using the generated cloud mask. With the help of drone image, a subset of Landsat data is created. The vegetation mask is then created, as shown in Fig. 4(a), using drone image and markings from ground survey. Drone image subset is segmented into segments of size corresponding to spatial resolution of Landsat data and gridded with 5×5 grids in each segment. Percentage of sparse and dense area in each segment of the image is computed by identifying grids in the segment as sparse or dense grid, using the knowledge from ground survey and close inspection of drone image. This information serves as ground truth, by which band for segregation of sparse and dense class is selected with the help of SI. Theoretically and by the use of SI, it is noted that SWIR1 (band 6) is best suited for this classification. Once the band is selected, the threshold is selected using an adaptive thresholding technique based on the image statistics and user-defined boundary conditions. The image is classified into sparse and dense areas using the obtained threshold, as shown in Fig. 4(b).

The confusion matrix in Table III suggests that the proposed technique is able to produce highly consistent classification results relative to the reference data, as producer accuracy of sparse and dense vegetation classes obtained are 90% and 83.87%, respectively. Producer accuracy depends upon the error of omission which should be as less as possible for better accuracy, and it can be seen from Table IV that percentages of omission error are low, i.e., 0.10% and 0.16% for sparse and dense classes, respectively. On the other hand, user accuracy corresponds to the error of commission which should also be as less as possible as in the case of producer accuracy. Commission errors obtained for both the classes are also low, i.e., 0.12% and 0.13%, as mentioned in Table IV. Therefore, user accuracy obtained are satisfactory, i.e., 87.80% and 86.66% for sparse and dense vegetation classes, respectively. User accuracy is a good parameter for accuracy assessment of a classifier as it provides the accuracy of the technique developed from the perspective of the user of the classified map. Moreover, OA and FAR are also computed and found out to be 87.32% and 16.13%, respectively, since a total of 62 pixels for both classes are classified correctly out of 71 pixels and only 5 pixels out of 31 pixels of dense vegetation class are being misclassified into sparse vegetation class.

B. Validation

The developed approach is then validated by applying it over a different image that is different by location and date of acquisition. Drone image Loc2A and Landsat image L8A are selected for this purpose, and a subset of L8A is taken for the same area as in Loc2A. The vegetation mask is obtained as discussed in Section III-C, and is shown in Fig. 7(a). Reflectance values of the SWIR1 band are extracted for the pixels in the mask. Mean and standard deviation of the selected pixels are calculated and used in the developed adaptive thresholding approach to determine the optimized value of n. For this image, the lower bound for OA ($\mathrm{lb_{OA}}$) is kept same as in the previous image, but the upper bound for FAR ($\mathrm{ub_{FAR}}$) is changed to 10% for convergence. Then, the image is classified using the threshold value obtained from the optimized n value and is shown in Fig. 7(b).

To determine the accuracy of the classified image, the drone image is segmented into the size of an individual pixel of the Landsat image and 5×5 grids are made. Each grid is identified for sparse or dense grid and percentage of the sparse and dense area within the segment is computed. Using this information, the L8A data are classified and accuracy is computed to be

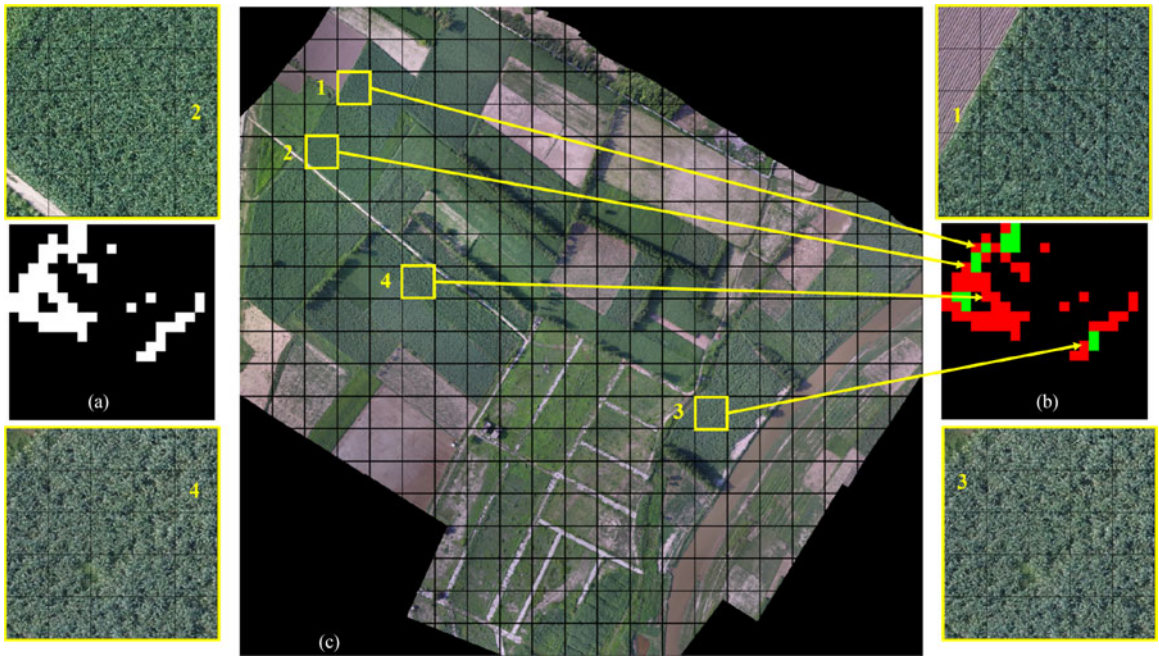

Fig. 7. Results for Loc2A of L8A subset: (a) vegetation mask (white represents sugarcane crop), (b) classified image (sparse (red) and dense (green)), and (c) drone image with grids of 30 m × 30 m with zoomed segments (1–4).

TABLE V
CONFUSION MATRIX FOR LOC2A OF L8A DATA

	Sparse#	Dense#	Total#	User Accuracy
Sparse#	39	13	52	75%
Dense#	4	9	13	69.2%
Total#	43	22	65	
Producer accuracy	90.7%	40.9%		73.8% (OA)

Number of pixels.

73.8% and presented in Table V. There are a total of 65 pixels in the vegetation mask for the classification of sugarcane field into sparse and dense areas. Out of which 43 pixels corresponds to sparse area and 22 pixels corresponds to dense area, as per our ground survey and careful inspection of drone data. Almost all the sparse pixels are classified correctly but some of the dense pixels are being misclassified as sparse. This is due to the location of dense pixels that lie in the neighborhood of sparse areas or at the contours of the fields.

Some of the misclassified dense pixels that lie in boundary of sparse class or boundary of field are marked in yellow boxes and their zoomed image segments are shown in the inset of Fig. 7(c). For example, Box 1 of the image is classified as sparse (Red dot in classified image Fig. 7(b)) but it is a dense region according to the ground truth. It may be due to its location at the boundary of the field next to barren land that is clearly seen in the zoomed image 1 in Fig. 7(c). Similarly, it can be observed in other zoomed images, such as 2, 3, and 4 in Fig. 7(c).

V. CONCLUSION

In this paper, an approach to segregate sparse and dense areas within a selected sugarcane field is developed and implemented. It uses the fusion of drone and satellite images for developing an adaptive approach by which the repetitive usage of drone could be minimized. The approach is made adaptive by using image statistics and finding threshold using a multiobjective optimization technique to maximize the OA and minimize the FAR. The results show that the approach has proven to be satisfactory for the classification between sparse and dense classes with an accuracy of about 87% and 73% for testing and validation data, respectively. To develop this algorithm the drone data are segmented into the spatial dimension of the satellite image and ground truth data are obtained by ground survey and careful inspection of gridded drone data. The proposed approach has a potential to be extended to different sensor data, as the developed approach is based on the image statistics. In the era of digital world, this approach may be quite useful and applicable to users, such as government agricultural agencies, policy makers, farmers, and also insurance agencies for Fasal Bima Yojana, India.

REFERENCES

[1] D. J. Mulla, "Twenty five years of remote sensing in precision agriculture: Key advances and remaining knowledge gaps," *Biosyst. Eng.*, vol. 114, pp. 358–371, Apr. 2013.
[2] A. McBratney, B. Whelan, T. Ancev, and J. Bouma, "Future directions of precision agriculture," *Precis. Agric.*, vol. 6, pp. 7–23, Feb. 2005.
[3] A. Baggio, "Wireless sensor networks in precision agriculture," in *Proc. ACM Workshop Real-World Wireless Sensor Netw.*, Stockholm, Sweden, 2005, pp. 1567–1576.
[4] N. Wang, N. Zhang, and M. Wang, "Wireless sensors in agriculture and food industry—Recent development and future perspective," *Comput. Electron. Agric.*, vol. 50, pp. 1–14, Jan. 2006.
[5] C. Zhang and J. M. Kovacs, "The application of small unmanned aerial systems for precision agriculture: A review," *Precis. Agric.*, vol. 13, pp. 693–712, Jul. 2012.
[6] D. Lu and Q. Weng, "A survey of image classification methods and techniques for improving classification performance," *Int. J. Remote Sens.*, vol. 28, pp. 823–870, Mar. 2007.

[7] P. Mishra and D. Singh, "A statistical-measure-based adaptive land cover classification algorithm by efficient utilization of polarimetric SAR observables," *IEEE Trans. Geosci. Remote Sens.*, vol. 52, no. 5, pp. 2889–2900, May 2014.
[8] T. Blaschke, "Object based image analysis for remote sensing," *ISPRS J. Photogramm. Remote Sens.*, vol. 65, pp. 2–16, Jan. 2010.
[9] Y. Shao, R. S. Lunetta, B. Wheeler, J. S. Iiames, and J. B. Campbell, "An evaluation of time-series smoothing algorithms for land-cover classifications using MODIS-NDVI multi-temporal data," *Remote Sens. Environ.*, vol. 174, pp. 258–265, Mar. 2016.
[10] N. R. Rao, P. K. Garg, and S. K. Ghosh, "Development of an agricultural crops spectral library and classification of crops at cultivar level using hyperspectral data," *Precis. Agric.*, vol. 8, pp. 173–185, Oct. 2007.
[11] M. Govender, K. Chetty, and H. Bulcock, "A review of hyperspectral remote sensing and its application in vegetation and water resource studies," *Water SA*, vol. 33, pp. 145–151, Jan. 2007.
[12] Y. Zhou *et al.*, "Mapping paddy rice planting area in rice-wetland coexistent areas through analysis of Landsat 8 OLI and MODIS images," *Int. J. Appl. Earth Obs. Geoinf.*, vol. 46, pp. 1–12, Apr. 2016.
[13] R. Molina, M. Vega, J. Mateos, and A. K. Katsaggelos, "Variational posterior distribution approximation in bayesian super resolution reconstruction of multispectral images," *Appl. Comput. Harmon. Anal.*, vol. 24, no. 2, pp. 251–267, 2008.
[14] S. Nakazawa and A. Iwasaki, "Super-resolution imaging using remote sensing platform," in *Proc. IEEE Int. Geosc. Remote Sens. Symp.*, 2014, pp. 1987–1990.
[15] S. Baker and T. Kanade, "Limits on super-resolution and how to break them," *IEEE Trans. Pattern Anal. Mach. Intell.*, vol. 24, no. 9, pp. 1167–1183, Sep. 2002.
[16] A. Turiel, H. Yahia, and C. J. Pérez-Vicente, "Microcanonical multifractal formalisma geometrical approach to multifractal systems: Part I. Singularity analysis," *J. Phys. Math. Theor.*, vol. 41, no. 1, 2007, Art. no. 015501.
[17] K. G. Nikolakopoulos, "Comparison of nine fusion techniques for very high resolution data," *Photogramm. Eng. Remote Sens.*, vol. 74, no. 5, pp. 647–659, 2008.
[18] S. Huang and F. Siegert, "Land cover classification optimized to detect areas at risk of desertification in North China based on SPOT VEGETATION imagery," *J. Arid Environ.*, vol. 67, pp. 308–327, Oct. 2006.
[19] K. McGwire, T. Minor, and L. Fenstermaker, "Hyperspectral mixture modeling for quantifying sparse vegetation cover in arid environments," *Remote Sens. Environ.*, vol. 72, pp. 360–374, Jun. 2000.
[20] C. Gevaert, "Combining hyperspectral UAV and mulitspectral FORM OSAT-2 imagery for precision agriculture applications," Master thesis, Lund Univ., Lund, Sweden, 2014.
[21] K. C. Swain *et al.*, "Adoption of an unmanned helicopter for low-altitude remote sensing to estimate yield and total biomass of a rice crop," *Trans. ASAE Amer. Soc. Agric. Eng.*, vol. 53, no. 1, pp. 21–27, 2010.
[22] J. A. J. Berni, P. J. Zarco-Tejada, L. Suarez, and E. Fereres, "Thermal and narrowband multispectral remote sensing for vegetation monitoring from an unmanned aerial vehicle," *IEEE Trans. Geosci. Remote Sens.*, vol. 47, no. 3, pp. 722–738, Mar. 2009.
[23] P. J. Hardin, M. W. Jackson, V. J. Anderson, and R. Johnson, "Detecting squarrose knapweed (Centaurea virgata Lam. Ssp. squarrosa Gugl.) using a remotely piloted Vehicle: A Utah case study," *GISci. Remote Sens.*, vol. 44, pp. 203–219, Sep. 2007.
[24] J. Primicerio *et al.*, "A flexible unmanned aerial vehicle for precision agriculture," *Precis. Agric.*, vol. 13, pp. 517–523, Aug. 2012.
[25] E. R. Hunt, M. Cavigelli, C. S. T. Daughtry, J. E. Mcmurtrey, and C. L. Walthall, "Evaluation of digital photography from model aircraft for remote sensing of crop biomass and nitrogen status," *Precis. Agric.*, vol. 6, pp. 359–378, Aug. 2005.
[26] "Landsat 8 (L8) Data Users Handbook," Department of the Interior U.S. Geological Survey, EROS, Sioux Falls, SD, USA, Mar. 2016.
[27] Z. Li, A. Khananian, R. H. Fraser, and J. Cihlar, "Automatic detection of fire smoke using artificial neural networks and threshold approaches applied to AVHRR imagery," *IEEE Trans. Geosci. Remote Sens.*, vol. 39, no. 9, pp. 1859–1870, Sep. 2001.
[28] W. C. Snyder, Z. Wan, Y. Zhang, and Y.-Z. Feng, "Classification-based emissivity for land surface temperature measurement from space," *Int. J. Remote Sens.*, vol. 19, no. 14, pp. 2753–2774, 1998.
[29] D. Murugan, A. Garg, T. Ahmed, and D. Singh, "Fusion of drone and satellite data for precision agriculture monitoring," in *Proc. 2016 IEEE 11th Int. Conf. Ind. Inf. Syst.*, Dec. 2016, to be published.
[30] J. Townshend, C. Justice, W. Li, C. Gurney, and J. McManus, "Global land cover classification by remote sensing: Present capabilities and future possibilities," *Remote Sens. Environ.*, vol. 35, pp. 243–255, Feb. 1991.
[31] N. Otsu, "A threshold selection method from gray-level histograms," *Automatica*, vol. 11, no. 285–296, pp. 23–27, 1975.
[32] R. S. Gautam, D. Singh, and A. Mittal, "An efficient contextual algorithm to detect subsurface fires with NOAA/AVHRR data," *IEEE Trans. Geosci. Remote Sens.*, vol. 46, no. 7, pp. 2005–2015, Jul. 2008.
[33] S. Agarwal and D. Singh, "An adaptive statistical approach for non-destructive underline crack detection of ceramic tiles using millimeter wave imaging radar for industrial application," *IEEE Sensors J.*, vol. 15, no. 12, pp. 7036–7044, Dec. 2015.

Deepak Murugan received the Bachelor's degree in Electronics and Communication Engineering from Anna University, Chennai, India, in 2008, and the M.Sc. degree in Electrical Engineering from Linköping University, Linköping, Sweden, in 2012. He has been working toward the Ph.D. degree in RF and microwave engineering in the Department of Electronics and Communication Engineering, Indian Institute of Technology Roorkee, Roorkee, India, since January, 2015.

His research interests include satellite based agriculture monitoring, SAR and optical data analysis, land cover classification, and soil moisture retrieval. He received a fellowship from RailTel, India, for his Ph.D. research work.

Akanksha Garg received the Bachelor's degree in Electronics and Communication Engineering from Rajasthan Technical University, Kota, India, in 2010, and the Master's degree in Microwave Engineering from the Indian Institute of Technology (Banaras Hindu University), Varanasi, India, in 2013. She has been working toward the Ph.D. degree in RF and microwave engineering in the Department of Electronics and Communication Engineering, Indian Institute of Technology Roorkee, Roorkee, India, since January, 2014.

Her research interests include polarimetry, SAR and optical data analysis, land cover classification, and resolution enhancement. She received a fellowship from the Ministry of Human Resource and Development, Government of India for her Ph.D. research work.

Dharmendra Singh (SM'10) received the Ph.D. degree in Electronics Engineering from Banaras Hindu University, Varanasi, India.

He has more than 21 years of experience in teaching and research. He was a Visiting Scientist Postdoctoral Fellow in the Department of Information Engineering, Niigata University, Niigata, Japan; the German Aerospace Center, Cologne, Germany; the Institute for National Research in Informatics and Automobile, France; the Institute of Remote Sensing Applications, Beijing, China; Karlsruhe University, Karlsruhe, Germany; and the Polytechnic University of Catalonia, Barcelona, Spain. He also visited several other laboratories in other countries. He is currently a Professor in the Department of Electronics and Communication Engineering, Indian Institute of Technology Roorkee, Roorkee, India, and a Coordinator at RailTel-IIT Roorkee Center of Excellence in Telecom, Roorkee, India. He has published more than 300 papers in various national/international journals and conferences. His research interests include microwave remote sensing, electromagnetic wave interaction with various media, polarimetric and interferometric applications of microwave data, and numerical modeling, ground penetrating radar, through wall imaging and stealth technology. He has received various fellowships and awards from national and international bodies.